

Electronic Supplementary Information (ESI)

**Highly sensitive detection of low-level water contents in
organic solvents and cyanide in aqueous media using novel
solvatochromic AIEE fluorophores**

Wei Chen,^a Zhiyun Zhang, ^a Xin Li,^{*b} Hans Ågren^b and Jianhua Su^{*a}

^a Key Laboratory for Advanced Materials and Institute of Fine Chemicals, East China University of Science & Technology, Shanghai 200237, P. R. China, Fax: (+86)-21-64252288, E-mail: bbsjh@ecust.edu.cn

^b Division of Theoretical Chemistry and Biology, School of Biotechnology, KTH Royal Institute of Technology, SE-10691 Stockholm, Sweden, E-mail: lixin@theochem.kth.se

Contents

| | |
|--|-----|
| 1. Solvatochromism | S2 |
| 2. Calculated vertical transition information and dipole moment | S3 |
| 3. Detection of low-level water | S4 |
| 4. AIEE behaviours and optimized geometries | S6 |
| 5. Detection of cyanide and supporting calculation | S7 |
| 6. ¹ H, ¹³ C NMR, HRMS and Crystal data for sensors and products | S11 |
| 7. Full Listing for Reference 74..... | S15 |

1. Solvatochromism

Table 1 Photophysical properties of **BDM** and **BDBM** in various solvents.

| Solvent ^a | Δf^b | $E_T^N c$ | BDM | | | | BDBM | | | |
|----------------------|--------------|-----------|----------------------------------|---------------------------------|-------------------------------------|-------------------|----------------------------------|---------------------------------|-------------------------------------|-------------------|
| | | | λ_{abs}^d (nm) | λ_{em}^e (nm) | Δv^f (cm ⁻¹) | Φ_F^g (%) | λ_{abs}^d (nm) | λ_{em}^e (nm) | Δv^f (cm ⁻¹) | Φ_F^g (%) |
| Cyc | -0.0016 | 0.006 | 407 | 539 | 6017 | 7 | 400 | 544 | 6618 | 6 |
| Hex | -0.0011 | 0.009 | 403 | 537 | 6192 | 5 | 400 | 541 | 6516 | 9 |
| Tol | 0.0132 | 0.099 | 396 | 580 | 8011 | 10 | 392 | 561 | 7685 | 11 |
| Dio | 0.0223 | 0.164 | 387 | 597 | 9089 | 8 | 385 | 572 | 8492 | 11 |
| Et ₂ O | 0.1641 | 0.117 | 393 | 607 | 8971 | 14 | 400 | 582 | 7818 | 10 |
| THF | 0.2096 | 0.207 | 389 | 615 | 9447 | 7 | 395 | 597 | 8566 | 6 |
| DCM | 0.2172 | 0.327 | 408 | 634 | 8737 | 3 | 404 | 606 | 8251 | 11 |
| DMSO | 0.2630 | 0.444 | 396 | 628 | 9329 | <1 | 392 | 641 | 9510 | 1 |
| BuOH | 0.2644 | 0.586 | 394 | 615 | 9121 | 1 | 404 | 617 | 8545 | 2 |
| MeCN | 0.3055 | 0.460 | 390 | 637 | 9942 | <1 | 395 | 630 | 9443 | 2 |

^a Abbreviations: Hex, n-Hexane; Cyc, Cyclohexane; Tol, Toluene; Dio, Dioxane; Et₂O, ethylether; THF, Tetrahydrofuran; DCM, Dichloromethane; DMSO, Dimethyl sulfoxide; BuOH, n-Butanol; MeCN, Acetonitrile.

^b $\Delta f = (\epsilon - 1)/(2\epsilon + 1) - (n^2 - 1)/(2n^2 + 1)$ accounts for the spectral shifts due to reorientation of the solvent molecules, called the orientation polarizability, where ϵ is solvent dielectric constant and n is index of refraction.

^c E_T^N , empirical parameters of solvent polarity.

^d λ_{abs} , absorption maximum wavelength.

^e λ_{em} , emission maximum wavelength.

^f Δv , Stokes shift.

^g Φ_F , fluorescence quantum yield.

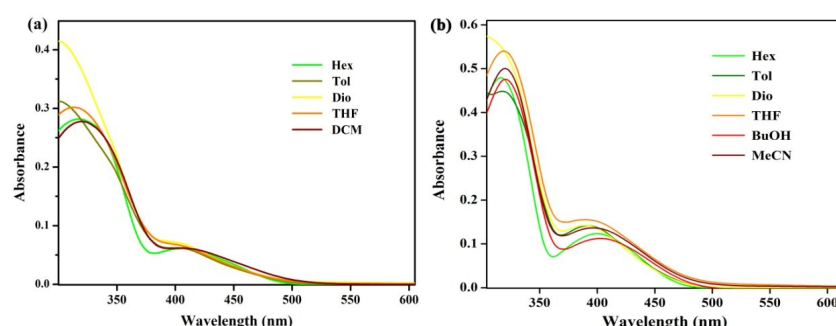


Fig. S1 Absorption spectra of (a) **BDM** and (b) **BDBM** in different solvents. Concentration: 10 $\mu\text{mol}\cdot\text{L}^{-1}$.

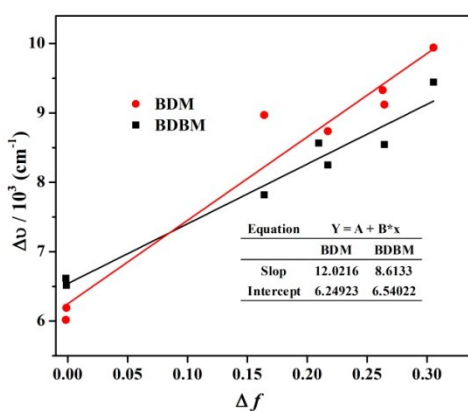


Fig. S2 Plot of Stokes shift (Δf) of **BDM** and **BDBM** versus Δv in different solvent.

2. Calculated vertical transition information and dipole moment

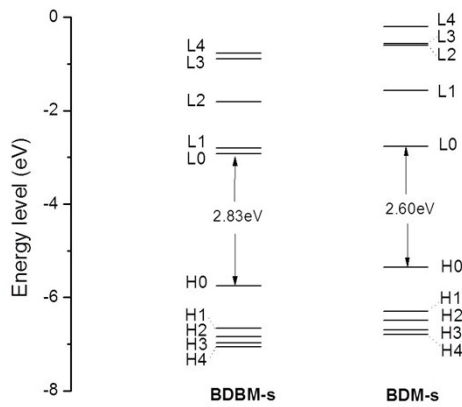


Fig. S3 Energy levels of frontier molecular orbitals of **BDBM** and **BDM**.

Table S2 Computed excitation energies, oscillator strengths and molecular orbital compositions of low-lying excited states of **BDBM** and **BDM**.

| Compound | State | Excitation energy | Oscillator strength (<i>f</i>) | MO composition |
|-------------|----------------|-------------------|----------------------------------|-----------------|
| BDBM | S ₁ | 2.90 eV, 426 nm | 0.1077 | H-0 → L+0 (83%) |
| | S ₂ | 3.24 eV, 382 nm | 0.5008 | H-0 → L+1 (93%) |
| | S ₃ | 3.82 eV, 324 nm | 0.3145 | H-1 → L+1 (29%) |
| | | | | H-2 → L+1 (25%) |
| | | | | H-0 → L+2 (18%) |
| | | | | H-5 → L+0 (11%) |
| BDM | S ₁ | 2.93 eV, 423 nm | 0.2107 | H-0 → L+0 (86%) |
| | S ₂ | 3.73 eV, 332 nm | 0.7414 | H-0 → L+1 (79%) |
| | S ₃ | 3.75 eV, 330 nm | 0.3755 | H-1 → L+0 (55%) |
| | | | | H-2 → L+0 (15%) |
| | | | | H-7 → L+0 (34%) |
| | | | | H-2 → L+0 (27%) |
| | | | | H-1 → L+0 (10%) |
| BDM | S ₄ | 4.14 eV, 299 nm | 0.0077 | H-3 → L+0 (20%) |
| | S ₅ | 4.33 eV, 286 nm | 0.0845 | H-7 → L+0 (19%) |
| | | | | H-1 → L+0 (17%) |
| | | | | H-5 → L+0 (12%) |
| | | | | H-6 → L+0 (11%) |

Table S3 The dipole moments in the ground (μ_g) and the first excited (μ_e) states for **BDM** and **BDBM**.

| | μ_g/Deby e | μ_e/Deby | $\square\mu_e - \mu_g)/\text{Deby}$ e |
|------------|--------------------------|---------------------|--|
| BDM | 9.7 | 22.9 | 13.2 |

| | | | |
|-------------|------|------|------|
| BDBM | 19.6 | 30.1 | 10.5 |
|-------------|------|------|------|

3. Detection of low-level water

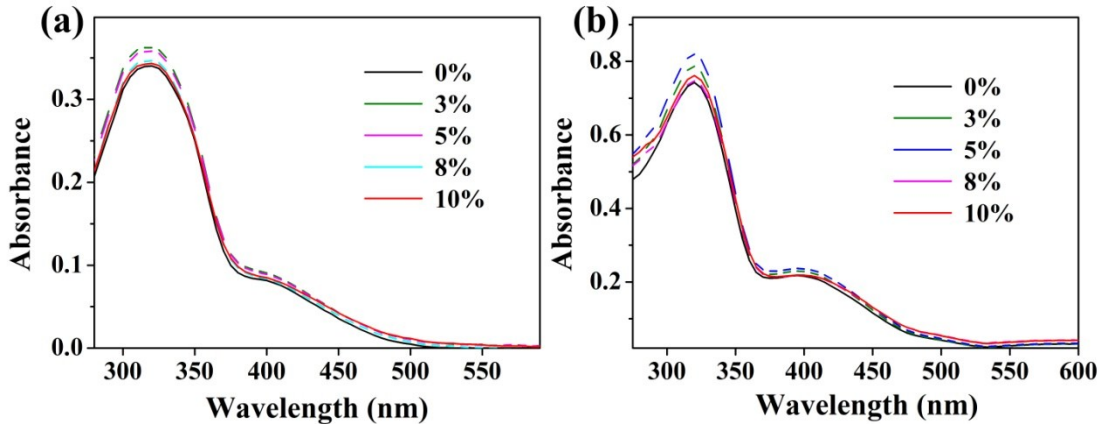


Fig. S4 Absorption spectra of (a) **BDM** and (b) **BDBM** in THF solution in the presence of increasing amount of water.

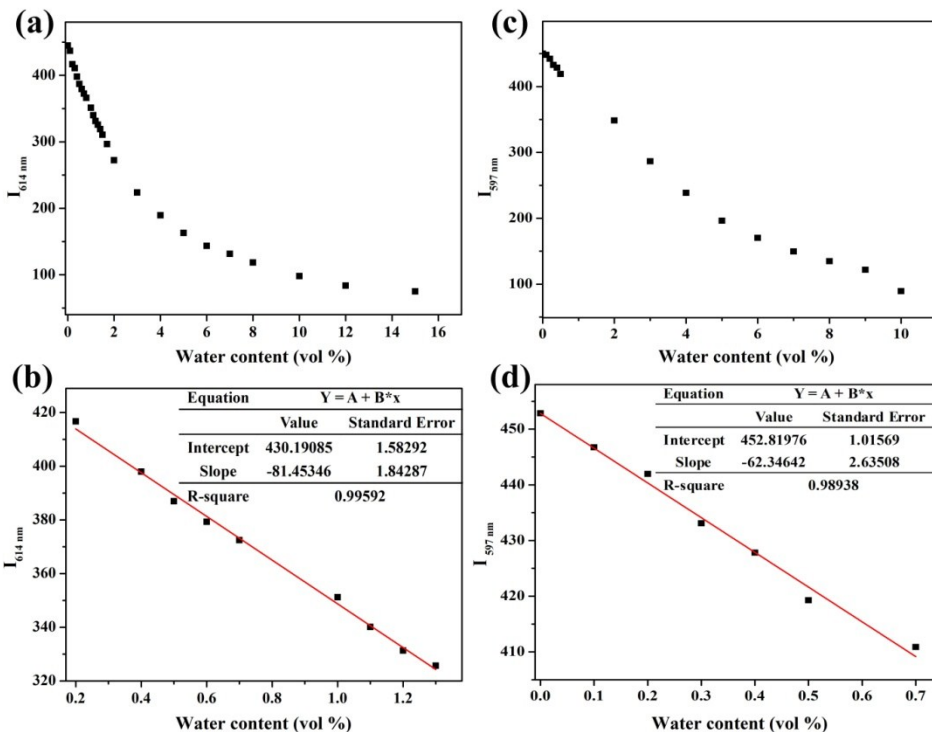


Fig. S5 (a) Fluorescent peak intensity of **BDM** at 614 nm in THF (a) and at 597 nm in dioxane (c) with increasing water content. (b) Plot of fluorescent intensity change of **BDM** versus varied concentrations of H_2O in THF solution. $\lambda_{ex} = 400$ nm, $\lambda_{em} = 614$ nm, $R^2 = 0.99592$, $k = -8145.3$, $\sigma = 0.28$. The Standard deviation (σ) was obtained by fluorescence responses (10-times of consecutive scanning on the Varian Cary Eclipse Fluorescence Spectrophotometer). The detection limit was calculated by the formula $(3\sigma/|k|)$ giving the result of 0.010%. (d) Plot of fluorescent intensity change of **BDM**

versus varied concentrations of H_2O in dioxane solution. $\lambda_{\text{ex}} = 400 \text{ nm}$, $\lambda_{\text{em}} = 597 \text{ nm}$, $R^2 = 0.98938$, $k = -6234.6$, $\sigma = 0.39$. The Standard deviation (σ) was obtained as aforementioned and the detection limit was calculated as 0.019%.

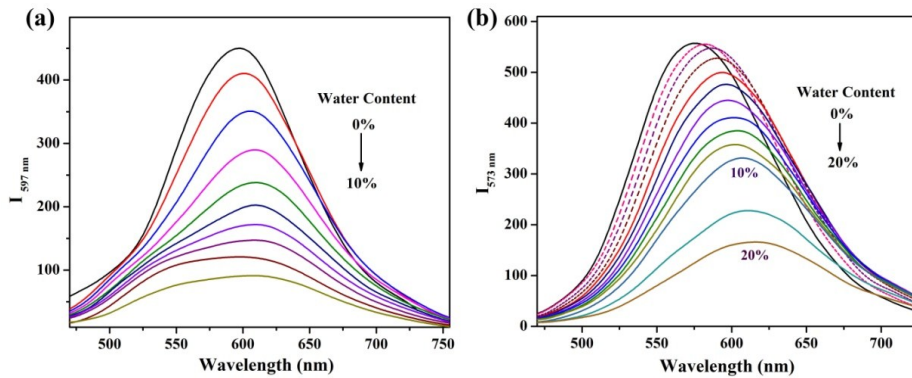


Fig. S6 Fluorescence spectra of (a) **BDM** and (b) **BDBM** in dioxane solution in the presence of increasing amount of water.

4. AIEE behaviours and optimized geometries

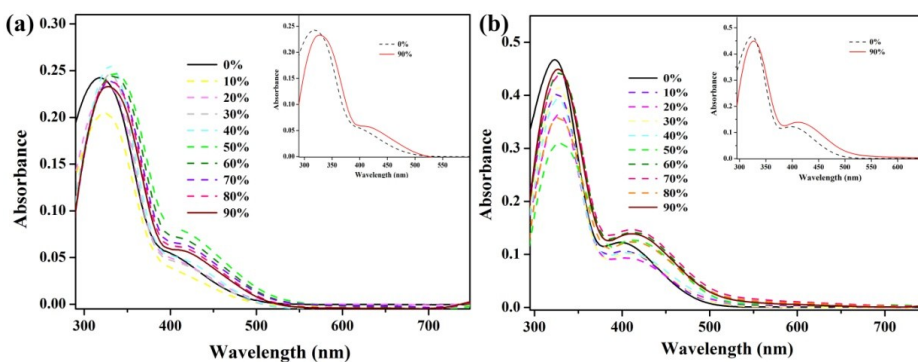


Fig. S7 Absorption spectra of **BDM** (a) and **BDBM** (b) in DMSO/water mixtures with different water contents. Concentration: 10 μ M.

Table S4 Computed free energies of the compounds.

| | Self-consistent field energy | Zero-point energy | Thermal correction | Relative free energy |
|---------------|------------------------------|-------------------|--------------------|----------------------------------|
| BDBM-s | -1837.60442530 a.u. | 0.600123 a.u. | 0.529692 a.u. | |
| BDBM-t | -1837.59839243 a.u. | 0.600331 a.u. | 0.526311 a.u. | 7.5 kJ/mol, w.r.t. BDBM-s |
| BDM-s | -1615.04011757 a.u. | 0.596619 a.u. | 0.531220 a.u. | |
| BDM-t | -1615.03486889 a.u. | 0.596881 a.u. | 0.528109 a.u. | 6.3 kJ/mol, w.r.t. BDM-s |

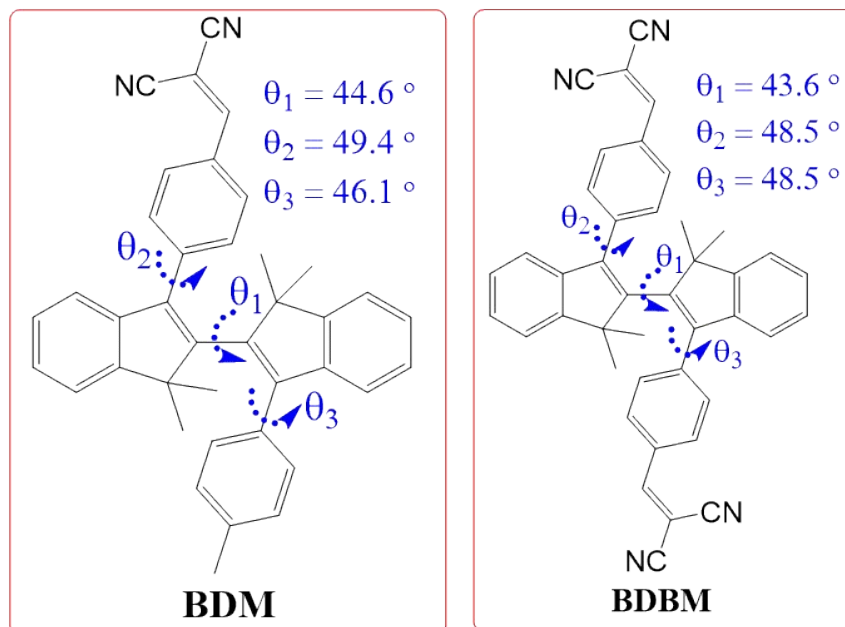


Fig. S8 Calculated dihedral angles of compound **BDBM** and **BDM**.

5. Detection of cyanide and supporting calculation

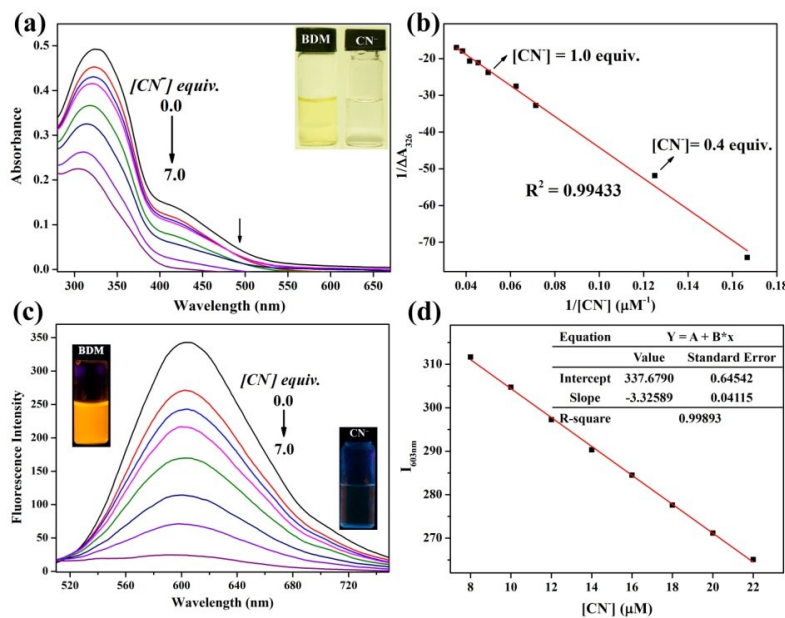


Fig. S9 (a) Absorption spectral changes of **BDM** ($20 \mu\text{M}$) upon the addition of 0-7.0 equiv. cyanide in 2 mM CTAB micellar solution. Insert: the images of **BDM** with different amount of cyanide (left: none; right: 7.0 equiv. cyanide). (b) Benesi–Hildebrand plot of absorbance at 326 nm. (c) Fluorescence spectra of **BDM** ($20 \mu\text{M}$) upon addition of 0-7.0 equiv. cyanide in 2 mM CTAB micellar solution. Insert: the images of fluorescence with different amounts of cyanide (left: none; right: 7.0 equiv. cyanide). (d) Plot of fluorescence intensity versus cyanide concentration, $\lambda_{\text{ex}} = 400 \text{ nm}$, $\lambda_{\text{em}} = 603 \text{ nm}$, $R^2 = 0.99893$, $k = -3.33 \mu\text{M}^{-1}$, $\sigma = 0.36$. The standard deviation (σ) was obtained by fluorescence responses (10-times of consecutive scanning on the Varian Cary Eclipse Fluorescence Spectrophotometer). The detection limit was calculated as $0.32 \mu\text{M}$ by the formula $(3\sigma/|k|)$.

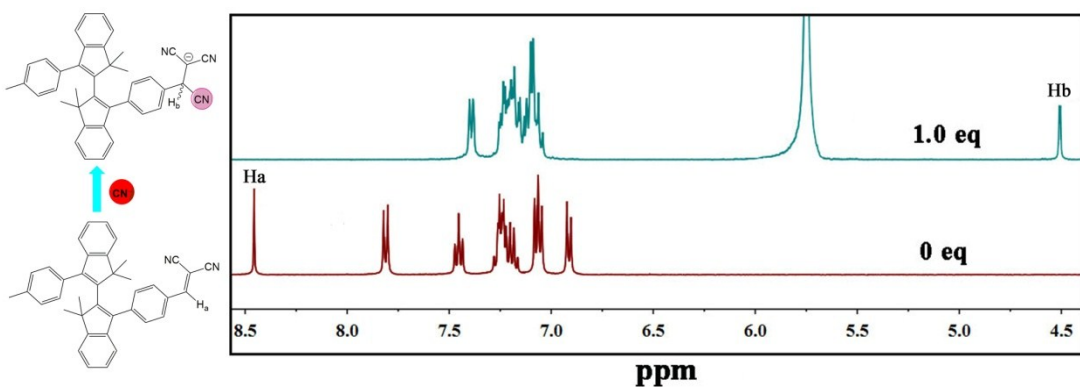


Fig. S10 ^1H NMR spectra of **BDM** in $\text{DMSO}-d_6$ upon addition of cyanide anion in CH_2Cl_2 .

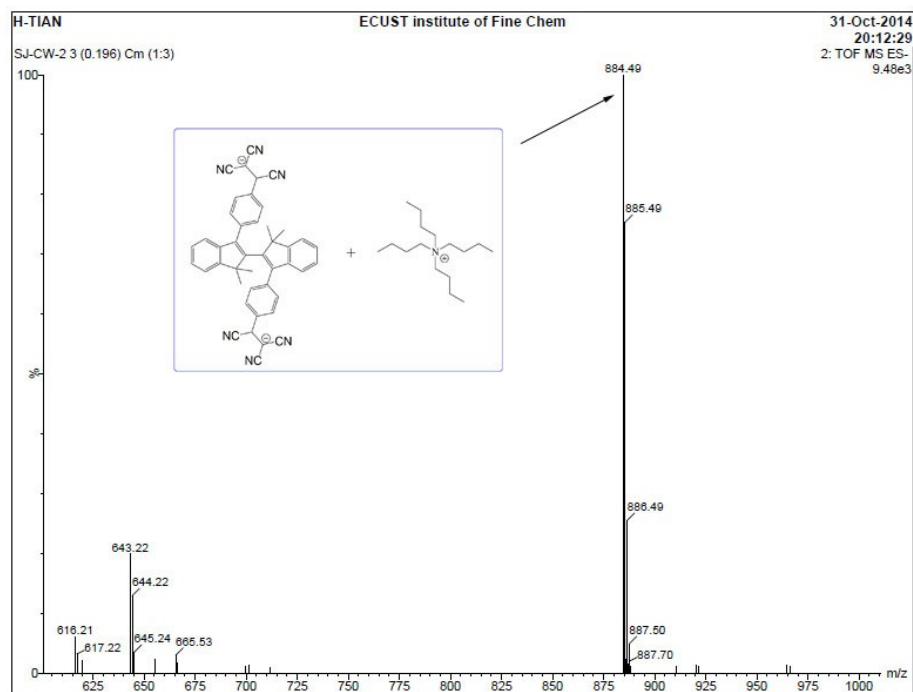


Fig. S11 MS (ESI-) spectrum of compound **BDBM** (10 μ M) with CN^- (25 μ M) in CH_2Cl_2 solution at 25 °C. Calcd for $\text{C}_{60}\text{H}_{66}\text{N}_7^- = 884.54$, found: 884.49.

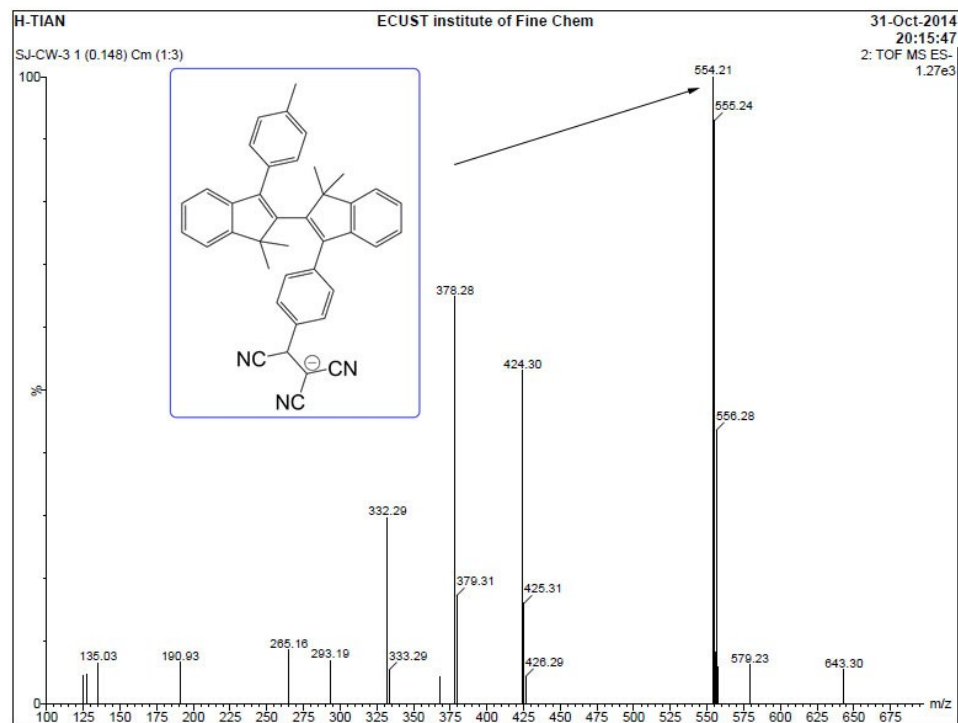


Fig. S12 MS (ESI-) spectrum of compound **BDM** (10 μ M) with CN^- (15 μ M) in CH_2Cl_2 solution at 25 °C. Calcd for $\text{C}_{40}\text{H}_{32}\text{N}_3^- = 554.26$, found: 554.21.

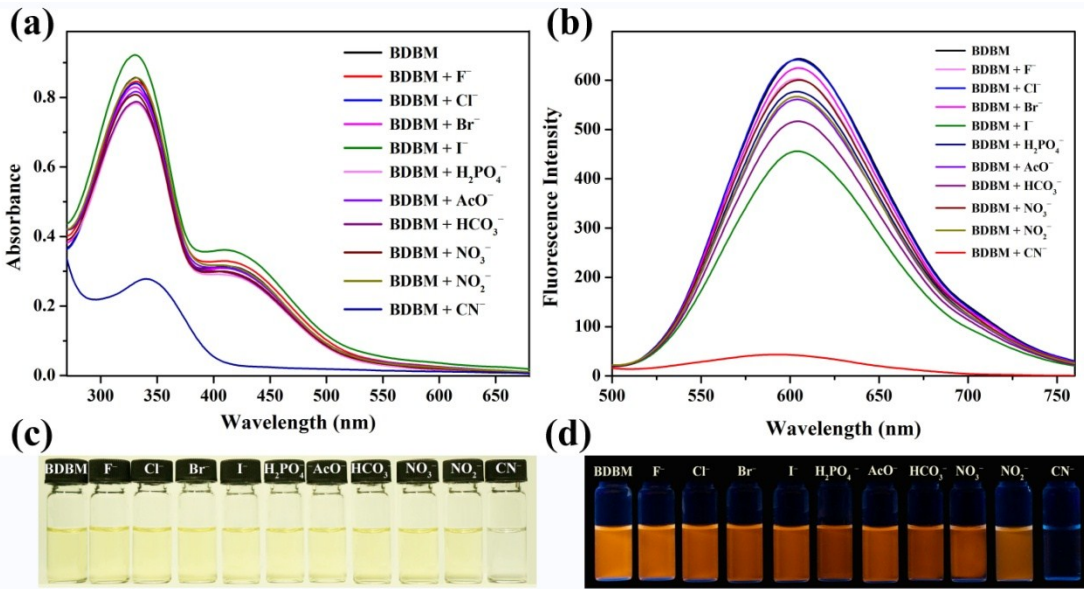


Fig. S13 (a) Absorption spectra and (b) fluorescence of **BDBM** in CTAB micelles (2 mM) upon addition of various anions (CN⁻: 9.0 equiv., other anions: 45.0 equiv.). The corresponding colour (c) and emission (d) changes of **BDBM** in CTAB micelles (2 mM) upon addition of various anions. Concentration: 20 μ M; excitation wavelength: 400 nm.

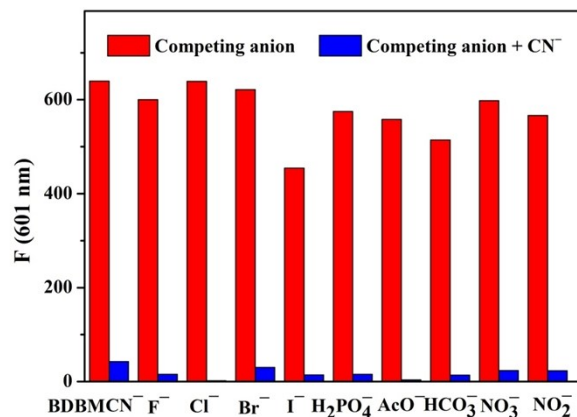


Fig. S14 The fluorescence intensity changes at 601 nm of **BDBM** (20 mM) upon addition of 9.0 equiv. of CN⁻ and 45.0 equiv. of various interference anions.

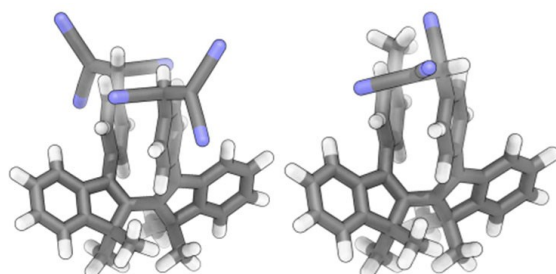


Fig. S15 Optimized geometries of (left) [CN-BDBM-CN]²⁺ and (right) [CN-BDM]⁻.

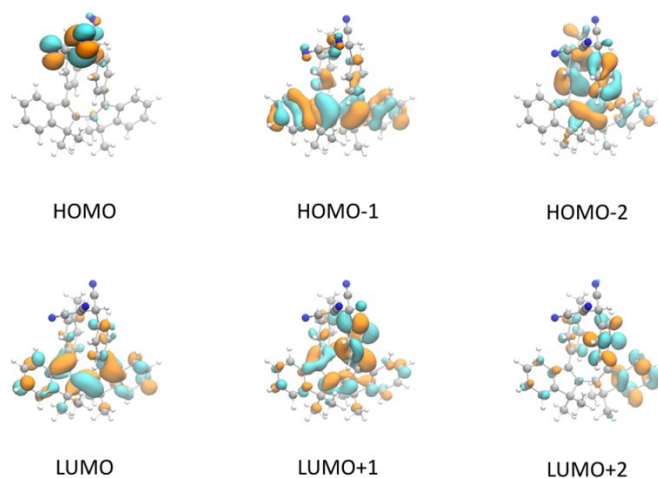


Fig. S16 Frontier molecular orbitals of $[\text{CN-BDM}]^-$.

Table S5 Computed excitation energies, oscillator strengths and molecular orbital compositions of low-lying excited states of $[\text{CN-BDBM-CN}]^{2-}$ and $[\text{CN-BDM}]^-$.

| Compound | State | Excitation energy | Oscillator strength (f) | MO composition |
|----------------------------|-------|-------------------|-----------------------------|---|
| $[\text{CN-BDBM-CN}]^{2-}$ | S_1 | 3.56 eV, 348 nm | 0.4597 | H-2 → L+0 (73%) H-0 → L+0 (21%) |
| | S_2 | 3.94 eV, 314 nm | 0.0201 | H-0 → L+1 (13%) |
| | S_3 | 3.94 eV, 314 nm | 0.0259 | H-1 → L+1 (13%) |
| | S_4 | 4.42 eV, 280 nm | 0.1482 | H-1 → L+0 (29%) H-0 → L+1 (22%) H-2 → L+1 (13%) |
| | S_5 | 4.46 eV, 277 nm | 0.0042 | H-2 → L+1 (50%) H-1 → L+0 (24%) |
| | | | | |
| $[\text{CN-BDM}]^-$ | S_1 | 3.47 eV, 356 nm | 0.3927 | H-1 → L+0 (87%) |
| | S_2 | 4.11 eV, 301 nm | 0.0025 | H-0 → L+16 (41%) |
| | S_3 | 4.31 eV, 287 nm | 0.0291 | H-0 → L+0 (63%) H-0 → L+1 (10%) |
| | S_4 | 4.57 eV, 271 nm | 0.0194 | H-2 → L+0 (38%) H-1 → L+1 (35%) |
| | S_5 | 4.63 eV, 267 nm | 0.1764 | H-2 → L+0 (42%) H-1 → L+1 (32%) |
| | | | | |

6. ^1H , ^{13}C NMR, HRMS and Crystal data for sensors and products

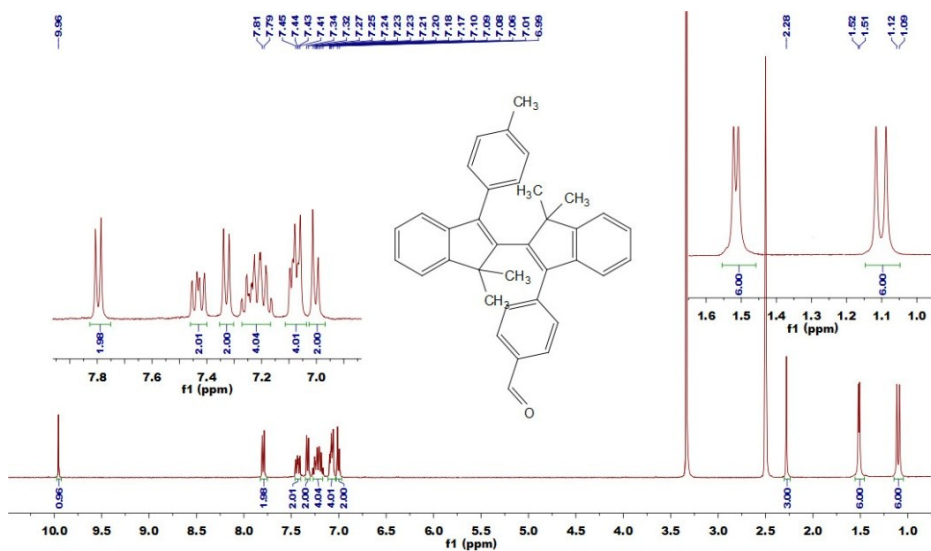


Fig. S17 ^1H NMR (400 MHz, $\text{DMSO}-d_6$) spectrum of compound 2.

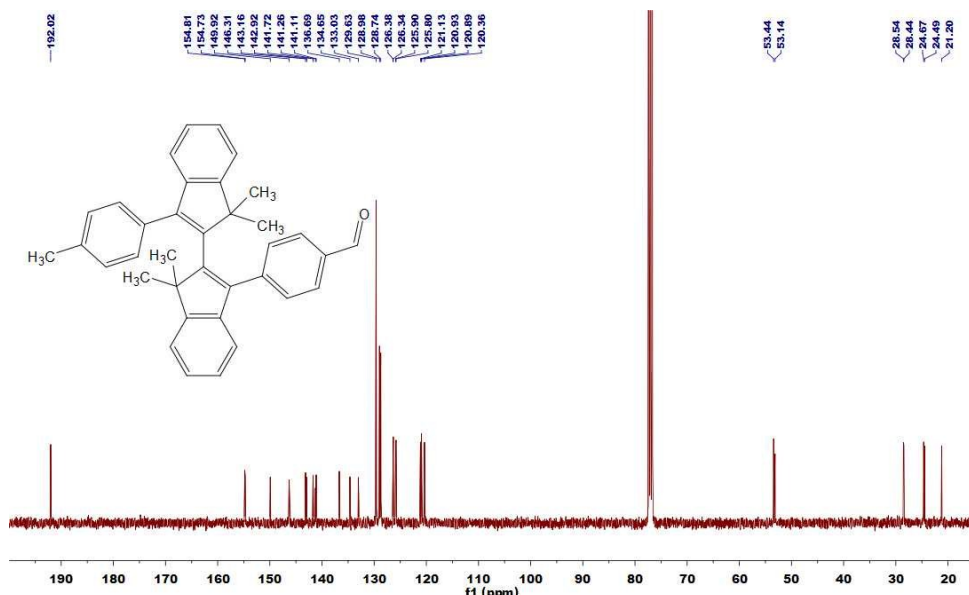


Fig. S18 ^{13}C NMR (100 MHz, CDCl_3) spectrum of compound 2.

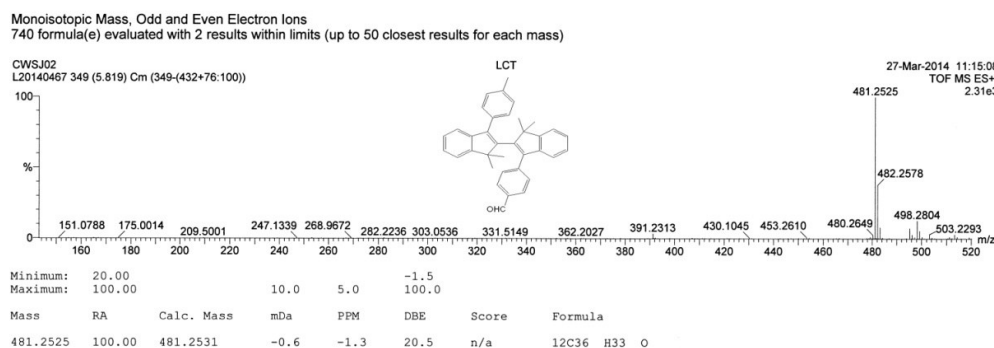


Fig. S19 ESI-MS spectrum of compound 2.

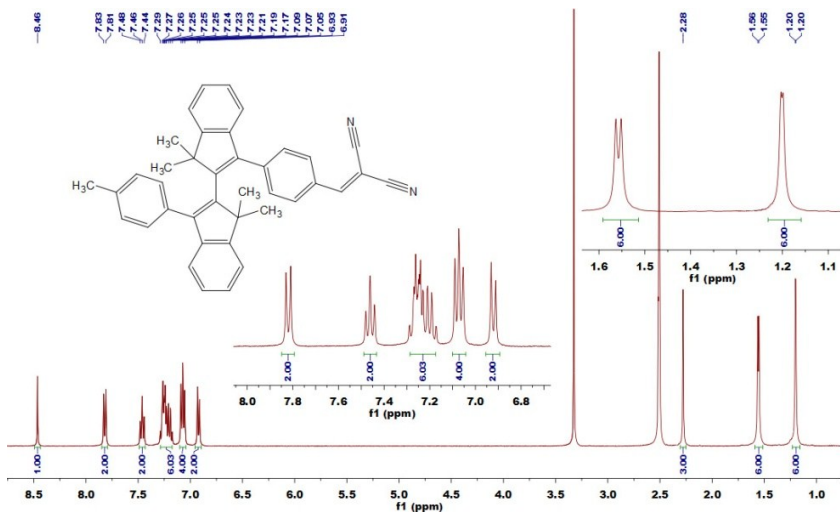


Fig. S20 ^1H NMR (400 MHz, DMSO- d_6) spectrum of compound **BDM**.

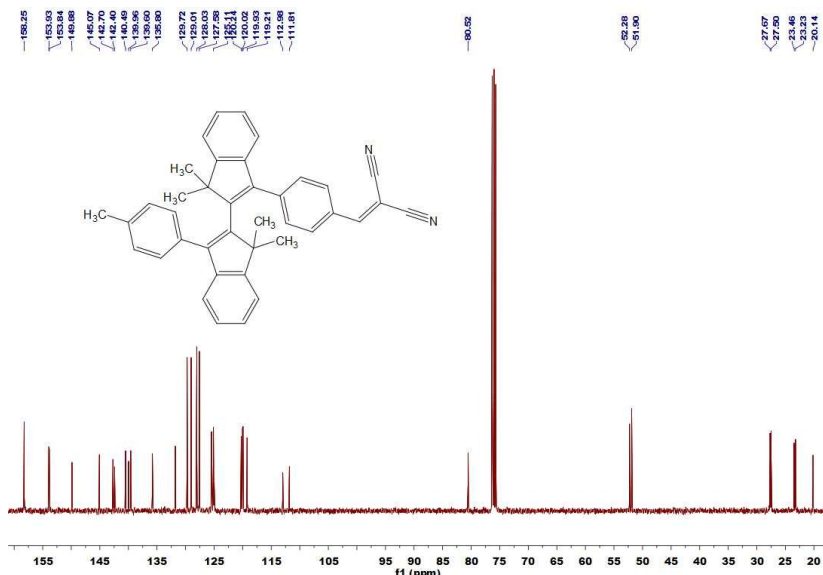


Fig. S21 ^{13}C NMR (100 MHz, CDCl₃) spectrum of compound **BDM**.

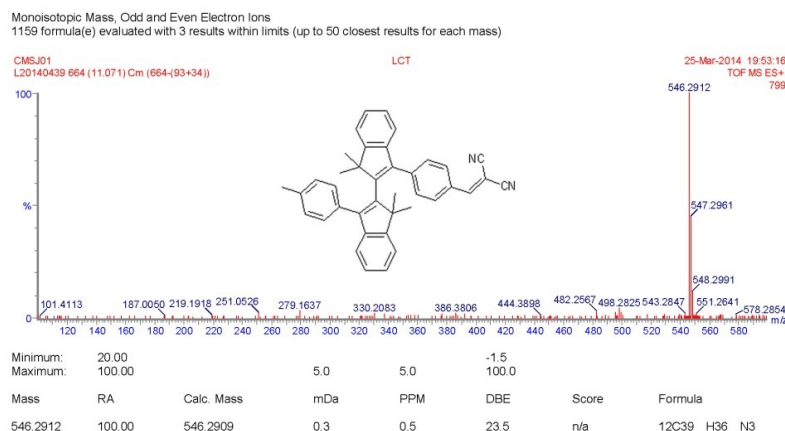


Fig. S22 ESI-MS spectrum of compound **BDM**.

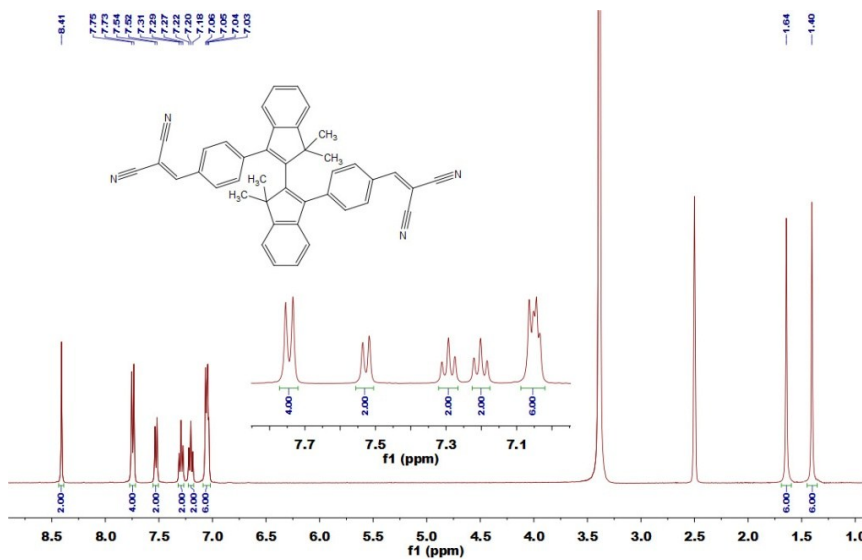


Fig. S23 ^1H NMR (400 MHz, $\text{DMSO}-d_6$) spectrum of compound **2**.

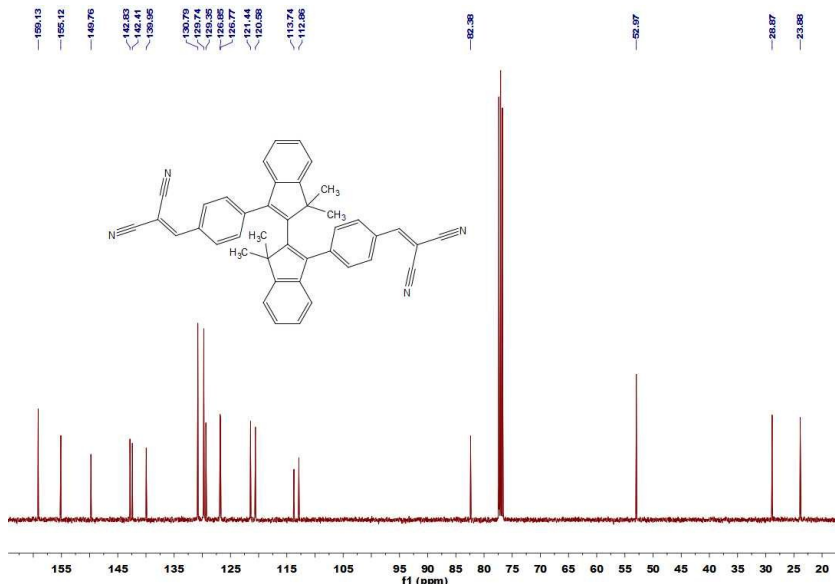


Fig. S24 ^{13}C NMR (100 MHz, CDCl_3) spectrum of compound **BDBM**.

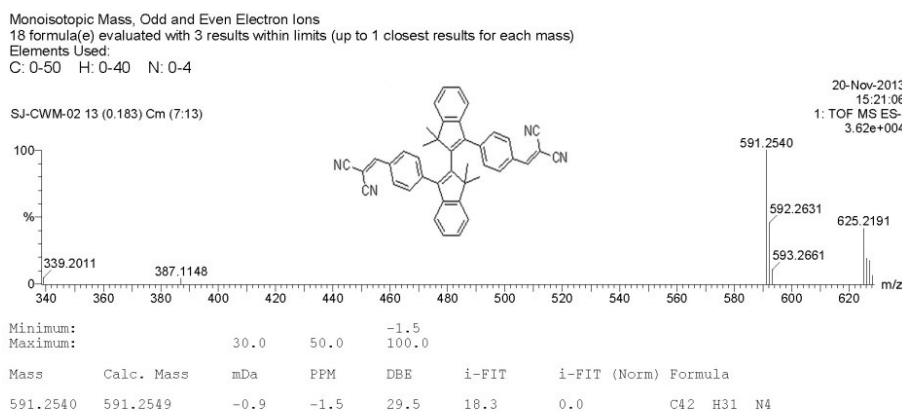


Fig. S25 ESI-MS spectrum of compound **BDBM**.

Table S6 Crystal data and structure refinement for compound **BDBM**.

| BDBM | |
|-----------------------------------|--|
| Empirical formula | C ₄₂ H ₃₀ N ₄ |
| Formula weight | 590.7 |
| Temperature | 293(2) K |
| Wavelength | 0.71073 Å |
| Crystal system | Monoclinic |
| Space group | C 2/c |
| a | 17.624(4) Å |
| b | 13.658(3) Å |
| c | 14.035(3) Å |
| α | 90° |
| β | 108.504(4)° |
| γ | 90° |
| Volume | 3203.8(11) Å ³ |
| Z | 4 |
| Density (calculated) | 1.225 Mg/m ³ |
| Absorption coefficient | 0.072 mm ⁻¹ |
| F(000) | 1240 |
| Crystal size | 0.211 x 0.175 x 0.123 mm ³ |
| Theta range for data collection | 1.926 to 25.999°. |
| Index ranges | -21<=h<=21, -16<=k<=16, -14<=l<=17 |
| Reflections collected | 9452 |
| Independent reflections | 3154 [R(int) = 0.0593] |
| Completeness to theta = 25.242° | 99.90% |
| Absorption correction | Semi-empirical from equivalents |
| Max. and min. transmission | 0.7457 and 0.6353 |
| Refinement method | Full-matrix least-squares on F ² |
| Data / restraints / parameters | 3154 / 0 / 211 |
| Goodness-of-fit on F ² | 1.032 |
| Final R indices [I>2sigma(I)] | R1 = 0.0643, wR ₂ = 0.1528 |
| R indices (all data) | R1 = 0.0799, wR ² = 0.1670 |
| Extinction coefficient | 0.0095(12) |
| Largest diff. peak and hole | 0.343 and -0.285 e.Å ⁻³ |
| CCDC number | 1016979 |

7. Full Listing for Reference 74

M. J. Frisch, G. W. Trucks, H. B. Schlegel, G. E. Scuseria, M. A. Robb, J. R. Cheeseman, G. Scalmani, V. Barone, B. Mennucci, G. A. Petersson, H. Nakatsuji, M. Caricato, X. Li, H. P. Hratchian, A. F. Izmaylov, J. Bloino, G. Zheng, J. L. Sonnenberg, M. Hada, M. Ehara, K. Toyota, R. Fukuda, J. Hasegawa, M. Ishida, T. Nakajima, Y. Honda, O. Kitao, H. Nakai, T. Vreven, J. A. Montgomery, Jr., J. E. Peralta, F. Ogliaro, M. Bearpark, J. J. Heyd, E. Brothers, K. N. Kudin, V. N. Staroverov, R. Kobayashi, J. Normand, K. Raghavachari, A. Rendell, J. C. Burant, S. S. Lyengar, J. Tomasi, M. Cossi, N. Rega, J. M. Millam, M. Klene, J. E. Knox, J. B. Cross, V. Bakken, C. Adamo, J. Jaramillo, R. Gomperts, R. E. Stratmann, O. Yazyev, A. J. Austin, R. Cammi, C. Pomelli, J. W. Ochtersk, R. L. Martin, K. Morokuma, V. G. Zakrzewski, G. A. Voth, P. Salvador, J. J. Dannenberg, S. Dapprich, A. D. Daniels, O. Farkas, J. B. Foresman, J. V. Ortiz, J. Cioslowski, D. J. Fox, *Gaussian 09*, revision A.2; Gaussian, Inc.: Wallingford CT, 2009.